Automated Design for Multi-Organ-on-Chip Geometries

Maria Emmerich, Philipp Ebner, *Student Member, IEEE* and Robert Wille *Senior Member, IEEE*

***Abstract*—Multi-Organs-on-Chips (multi-OoCs) represent human or other animal physiology on a chip—providing testing platforms for the pharmaceutical, cosmetic, and chemical industries. They are composed of miniaturized organ tissues (so-called organ modules) that are connected via a microfluidic channel network and, by this, represent organ functionalities and their interactions on-chip. The design of these multi-OoC geometries, however, requires a sophisticated orchestration of numerous aspects, such as the size of organ modules, the required shear stress on membranes and subsequently the flow rate, the dimensions and geometry of channels, pump pressures, etc. Mastering all this constitutes a non-trivial design task for which, unfortunately, no automatic support exists yet. In this work, we propose a design automation solution for multi-OoC geometries. To this end, we review the respective design steps and derive a corresponding formal design specification from them. Based on that, we then propose an automatic design tool, which generates a design of the desired device and exports it in a fashion that is ready for subsequent simulation or fabrication. The open-source tool and a step-by-step tutorial are available at https://github.com/cda-tum/mmft-ooc-designer. Evaluations (inspired by real-world use cases and confirmed by CFD simulations as well as a fabrication process) demonstrate the applicability and validity of the proposed approach.**

***Index Terms*—microfluidics, microphysiological system, organ-on-chip, physiological perfusion, shear stress, multi-organ, design automation**

I. Introduction

In 2022, the FDA updated the FD&C Act and, for the first time, allowed alternatives to animal testing for the approval of pharmaceuticals in the USA, specifically *Organs-on-Chips* (OoCs).

OoCs (also known as *Microphysiological Systems* , MPS) represent parts of the human physiology on-chip—providing an *in vitro* testing system. However, while culturing organs in a single tissue chip can provide insights into the mechanism within that single organ, intra-body communication and response to disease, injury, and therapy can only be investigated if a *combination* of organ modules is considered [1]. These *multi-OoCs* typically consist of several *organ modules* that include miniaturized organs and that are connected in a physiologically relevant fashion to other organ modules. Each organ module consists of a tank that holds some type of miniaturized scaffold and cells. The latter can include, e.g., lab-grown tissues [1], [2], organoids [3], bio-printed [4], [5], or patient-derived tissues such as tumor tissue [6], and simulate key aspects of human or other animal organs or organ units.

The connection between those organ modules is achieved via a *microfluidic channel network*. This allows for a fluid flow that interconnects the modules and supplies the cells with nutrients, removes waste, and realizes inter-organ communication via messenger molecules [7]. For the multi-OoC to mimic the reaction and effect on the represented organism, a well defined physical microenvironment within its modules and a circulating fluid flow are required [3], [8]. This organ communication from and between the organ modules occurs, *inter alia*, through cytokines (messenger molecules that allow inter-organ communication).

In some OoCs, a porous or semi-permeable *membrane* is employed to separate the cells from the microfluidic channel network. This membrane represents the endothelium, i.e., the inner lining of blood and lymph vessels of the organism on-chip, and emulates the organ tissue-blood barrier. It is usually seeded with endothelial cells, which results in more realistic drug absorption, distribution, metabolism, excretion, and toxicity [1], [9].

By this, OoCs provide the missing link between simple, ordinary cell culture approaches, in which pharmaceutical compounds are first identified, and clinical trials by either supplementing or replacing animal studies.

At the moment, multi-OoCs geometries realize the interactions between organ modules either through (1) distinctive predefined systems [10], [11] (that are static and designed for a fixed combination of organs) or (2) plug-and-play connection systems [1], [12], [13] (that are more flexible and can realize different combinations of organs).

However, the design of the case dependent chip geometries is not a trivial task and requires a sophisticated orchestration of numerous aspects, such as the size and scaling of organ modules, the required shear stress on membranes, the dimensions and geometry of channels, pump pressures, etc. These aspects are correlated, and even slight changes can affect the whole system. Moreover, because of the various applications of multi-OoC systems, the testing of compounds, e.g., for patient-specific applications (testing a treatment on a platform with patient-derived tissues prior to treatment of the patient), requires frequent redesigns—leading to severe design and fabrication loops. Considering that the design of multi-OoC geometries has been conducted manually thus far, this leaves a tedious, error-prone, and costly process.

In this work[1], we propose techniques and methods that address these problems. To this end, we utilize expertise from the *design automation* domain and apply them to multi-OoC design requirements. Design automation was historically applied to the design of electrical circuits and systems—allowing

[1]A preliminary version of this work was published at the DATE Conference 2024 [14].

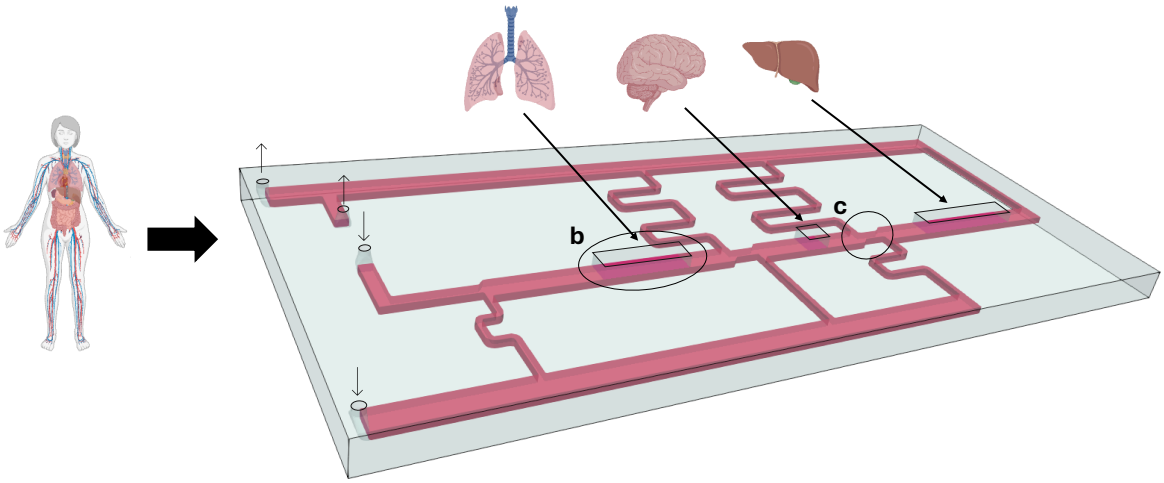

(a) Organ-on-Chip schematic with three organ modules (lung, brain, liver).

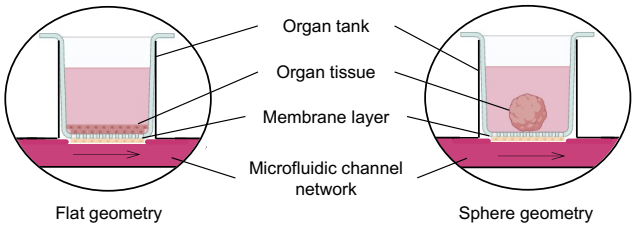

(b) Organ module schematics including membranes seeded with endothelial cells and tissue geometry.

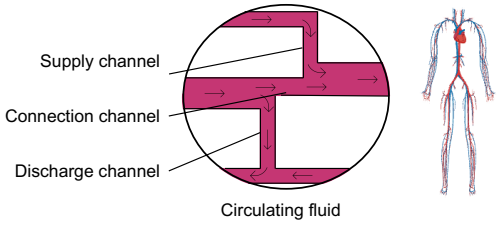

(c) Branching of the microfluidic channel network between organ modules.

Fig. 1: Multi-Organ-on-Chip schematic, partially created with biorender.com.

to realize the state-of-the-art IT systems composed of millions of components we take for granted today. In an effort to utilize those accomplishments for multi-OoC geometry design, we first review the respective design steps and then derive a corresponding formal specification from them. This formal specification is then used as input for a design automation approach generating the desired design. Finally, the obtained design is exported as a geometry definition that can directly be used in simulations or for subsequent fabrication.

The applicability and validity of the proposed approach are confirmed by evaluations. More precisely, the automatically generated designs for multi-OoC geometries are simulated, and one instance was fabricated using a commercially available 3D printer. The simulations confirm the validity of the tool, while the execution of the fabrication flow allowed to validate the usefulness of the resulting geometries for fabrication.

The remainder of this work is structured as follows: Section II reviews the general design of multi-OoCs. Afterwards, Section III introduces constraints to automatically define such a design. Section II describes the design method the resulting tool is based on, and in Section V the evaluations based on simulations and fabrication are summarized. Finally, Section VI concludes this work.

II. Design of Multi-Organ-on-Chips

At first glance, the design of multi-OoC geometries may look simple: Organ modules (for which several solutions have been proposed and fabricated in the past) [10], [15], [16] have to be taken and connected by a microfluidic channel network. However, the realization of (1) the correspondingly needed interplay between different organ modules, (2) the microfluidic channel network, and (3) the membranes that connect both is a non-trivial task. In this section, we briefly review the correspondingly needed design steps. To this end, we first revisit the overall structure of the corresponding devices. Afterwards, we cover how to properly design them.

A. Schematic of a Multi-Organ-on-Chip

Fig. 1a sketches the overall schematic of a multi-OoC. It includes organ modules, a microfluidic channel network, and membranes connecting both.

The overall design is based on the systemic connection of multiple organs on-chip, where the organ size is influenced by the chip design. The media perfusion is circulatory to mimic soluble factor cross-talk between the organs and unidirectional, but the media is also continuously replenished. Similar multi-OoC set-ups have been described in [1], [9], [17]–[20]. This physiologically relevant connection needs to be designed to replicate the complexity of the human body, influencing microgradients, exposure of organs, and is dependent on reasonably scaled organ sizes. This in turn drives the overall complexity of the channel network design.

1) Organ Modules: The organ modules represent the physiology on-chip by emulating the represented organism's organs. In Fig. 1b, examples of how organ modules can look are sketched. They contain organ tissues that are cultured in

tanks filled with a cell culture medium. The tissues inside of them can be one of two geometries: a sphere geometry or a flat geometry. The former represents suspended tissues like spheroids, organoids, or 3D structures (e.g., due to an artificial extracellular matrix; ECM). Typical examples include tumor tissues, but other organs like brain tissue can also be represented this way [21]. The flat geometry represents cell layers that grow directly on the epithelial membrane. Typical examples include barrier tissues such as the lung or skin [1], [9], [22]. The organ modules are often individually separated from the rest of the chip via a membrane.

2) Membranes: The membranes connect each organ module to the microfluidic channel network. They can be seeded with endothelial cells to simulate a vascular system. It realizes the cytokine and molecule exchange between each organ module and the microfluidic network, enabling the inter-organ communication between the modules.

3) Microfluidic Channel Network: Finally, the microfluidic channel network connects the different organ modules and, by this, allows for inter-organ communication. In Fig. 1c, a junction of the microfluidic channel network is depicted. Here, a *supply channel* is realized, which (through the inlet) introduces fresh cell culture medium (fluid) and, by this, new nutrients into the system (and, hence, to the organ modules). Vice versa, a *discharge channel* is realized, which (through the outlet) removes the fluid (now depleted cell culture medium), including any produced waste products, from the system. Conveniently, this can then also be used for subsequent analyses. Both the supply channel and the discharge channel have to employ the same flow rate (realized by the pumps) in order to keep the system in equilibrium. Additionally, a recirculation pump ensures that part of the discharge fluid is redirected back towards organ modules. Finally, a *connection channel* directly connects one organ module to the next organ module.

B. Design

To properly design multi-OoCs as reviewed above, several constraints have to be considered—constituting a non-trivial design. These constraints are reviewed in the following.

1) Organ Module Design: Each organ module consists of a tank in which a tissue is housed. In order to properly design a combination of organ modules, the relative sizes of the modules and the size of the tissues in them need to be proportional (since their relationship to each other and their impact on the system should be replicated the same way they interact in the represented organism) [9]. At the same time, the organ size of non vascularized tissues is restricted to a width of maximal 500 μm (depending on the cell type) [2], [21], [23]. In a larger tissue, the lack of vascularization would, therefore, lead to a lack of oxygen as well as nutrients and, hence, necrosis in the organ center. Defining the size of the organ modules also directly affects the design of the remaining multi-OoC geometry.

2) Membrane Design: The membrane, or, more precisely, the endothelial cells growing on the membrane, need to be exposed to a mechanical force, specifically a dedicated shear stress. That is, the tangential force that is applied to the endothelial layer should be low enough to not wash away the endothelial cells that are growing on the membrane. At the same time, it should replicate the shear stress of the represented organism (e.g., the blood flow along the vessel walls) to prevent dedifferentiation [24], i.e., the loss of cellular characteristics [25]. This, in turn, also affects, e.g., the required flow rate in the microfluidic channel network.

3) Microfluidic Channel Network Design: The microfluidic channel network connects the organ modules via the membranes on-chip. With that, it is key that this network is designed properly to achieve the desired physiological inter-organ communication. More precisely, the dimensions and geometry of the channels, as well as the realization of the respective branching, eventually regulate the flow rates of each channel. This, in turn, realizes the physiological perfusion *in vitro* and, by this, the rate of blood flow (emulated by the fluid within this microfluidic channel network) passing by the organ modules, which reproduces tissue exposure. Properly defining those flow rates is required to ensure that, e.g., organs with a lower perfusion are exposed to a lower volumetric flow rate, while organs with high perfusion, like the liver, are exposed to a larger flow rate. This, together with the size of the modules and the respective required shear stress to be realized on the membranes, requires a careful design of the entire network.

Overall, in order to properly design a multi-OoC including the microfluidic network geometry and the placement and extent of the organ modules, a sophisticated orchestration of numerous aspects is required, including the size and geometry of organ modules, the required or allowed shear stress acting on the membranes, the dimensions and geometry of the microfluidic channel network, and pump pressures, etc. Eventually, this results in various constraints that need to be considered when generating a corresponding design.

Resolving all these interlinked aspects is a complex task that is mainly conducted manually thus far. Accordingly, the design of corresponding devices still remains a tedious, error-prone, and costly task that urgently requires automation.

In the next two sections, we first derive a formal specification of the resulting multi-OoC geometry requirements and, then, propose a design approach that handles these tasks in an automated fashion.

III. Formal Specification

To determine a formal specification of the desired multi-OoC geometry, the aspects that were reviewed in the previous section need to be formalized. Again, this includes the specification of the organ modules, the required or allowed shear stress acting on the membranes, and their connection via the microfluidic channel network. The latter is responsible for representing the *physiological perfusion* of the organ modules and subsequently their exposure and effect to the whole system represented by the multi-OoC.

A. Organ Module Size and Geometry

First, the organ modules need to be defined. This includes the specification of its *tissue geometry* and *size*. In general, organ-on-chip systems usually employ two different types of

organ tissue geometries: spherical and flat tissues (as reviewed above and shown in Fig. 1b). However, more complex tissue structures can also be integrated in the organ modules. While the method defines the overall tissue and tank size, it does not necessarily define the tissue shape, allowing for flexibility in incorporating different tissue structures within the specified tank dimensions. For this, one of the two geometries—flat or sphere—needs to be selected based on which fits best the desired tissue configuration, as this choice determines the organ tank size calculation.

If only flat, i.e., layered, tissues are used, the channel width that is equal to the module width is set to $1\,\mathrm{mm}$. If, instead, at least one round tissue is included in the OoC, its radius r defines the module size and, hence, the circulating fluid channel width. More precisely, then, the organ module width and length are equal to $4 \times r$ where $r \leq 250\,\mu\mathrm{m}$ [21]. By including a distance of r from the tissue to the tank walls, the tissue can easily fit into the tank. This also allows for cell growth of the tissue and provides space for additional support structures that may be needed for tissue specifications. Furthermore, the organ cells are typically matured and exhibit slow growth rates [26], or they grow within the structures in which they are housed.

The organ module sizes need to be adjusted in relation to each other so that they indeed represent a scaled-down version of the considered organism. For this, a linearly scaling approach was employed, which results in the same mass (and volume) relation on-chip as in the represented organism. More precisely, when the mass of the complete scaled down organism M_b [kg] ("total mass of the miniaturized organism") is unknown, it can be determined by specifying the desired mass of the miniaturized organ module M_m [kg] using

$$M_b = \frac{M_m \times M_h}{M_{Tissue}}, \tag{1}$$

where M_h [kg] is the mass of a reference human and M_{Tissue} [kg] is the reference mass of the tissue in the reference human. Based on that, the weight of all remaining organ modules can be determined using

$$M_m = \frac{M_{Tissue} \times M_b}{M_h}. \tag{2}$$

Together, organ geometry and mass (and volume) define the module size and also influence the specification of the channel width and geometry of the microfluidic channel network. Any organ tissues growth is limited to the organ module tank and will not influence the fluid flow in the microfluidic channel network.

Of course, variations in the reference can be included to appropriately scale, e.g., with respect to sex or *Body Mass Index* (BMI), the desired chip. Appropriate values can be found in [27]–[29].

Example 1. *A typical organ module in a multi-OoC is a liver module. The size of the liver of a standard human male (*$70\,\mathrm{kg}$*) is* $1\,\mathrm{kg}$ *[30]. In a miniaturized liver-on-chip that simulates the liver of an organism with a weight of* $1e{-}6\,\mathrm{kg}$*, the liver organoid would have a mass of approx.* $1.42e{-}8\,\mathrm{kg}$*. This results in an organ module length of* $89\,\mu\mathrm{m}$ *at a width of* $1\,\mathrm{mm}$ *and a tissue height of* $150\,\mu\mathrm{m}$*.*

B. Shear Stress on Membrane

The endothelial layer that separates the organ modules from the circulating blood surrogate needs to be exposed to continuous shear stress τ [Pa] that is low enough to not wash away the endothelial cells growing on the membrane.

At the same time, it should replicate the shear stress of the represented organism, which needs to be strong enough to prevent dedifferentiation (loss of cellular characteristics). This means the shear stress should be between $1\,\mathrm{Pa}$ to $2\,\mathrm{Pa}$ [25]. Again, this can, of course, be adapted to fit the desired experimental characteristics by adapting the template.

To make sure the shear stress remains within this range, it can be controlled by the flow rate

$$Q = \frac{\tau \times w_{channel} \times h_{channel}^2}{6 \times \mu}, \tag{3}$$

where $w_{channel}$ [m] is the channel width of the channel that is connected to the organ module, $h_{channel}$ [m] its channel height, and μ [Pa s] is the dynamic viscosity of the circulating fluid [3]. The flow rate can later be experimentally controlled, and the required pump rates are an output of the presented automation method, while the channel height and viscosity can be set as a tool input. In the design approach and subsequent simulations, we assume that the cell layer and membrane do not impede fluid flow and are treated as a standard channel wall.

Example 2. *Consider the liver-on-chip described above. The membrane and the endothelial cells growing on it connect the liver module to the microfluidic channel network. The portal vein that transports blood through the liver has a wall shear stress of typically* $10\,\mathrm{dynes/cm^2}$ *to* $20\,\mathrm{dynes/cm^2}$ *[31]. To calculate the required flow rate in the channel below the organ module, we take the average shear stress in SI units, which is* $1.5\,\mathrm{Pa}$*, the channel width of* $1\,\mathrm{mm}$*, the channel height of* $150\,\mu\mathrm{m}$ *and the dynamic viscosity* $7.33\,\mathrm{e{-}4Pas}$ *of the common commercial culture media – Dulbecco's Modified Eagle Medium (DMEM) [32]. The resulting flow rate is* $7.71\,\mathrm{e{-}9\,m^3/s}$*. Based on this, the flow rates of the respective inflow and outflow of the connected channels can be calculated.*

C. Physiological Perfusion via the Microfluidic Channel Network

The physiological perfusion plays a significant role in the physiological relevance of the model. It describes the rate of blood flow through a tissue and is represented by the fluid flow in the microfluidic channel network of a multi-OoC. In the model, it is described by a physiological perfusion factor $perf$ that resembles the fraction of circulating fluid that is exchanged between the organ modules. The higher the perfusion, the higher the exposure of the organ module to the circulating fluid. This percentage is determined by

$$perf = \frac{Q_{organblood}}{Q_{totalblood}} \times \frac{V_{circ.fluid}}{V_{blood}}, \tag{4}$$

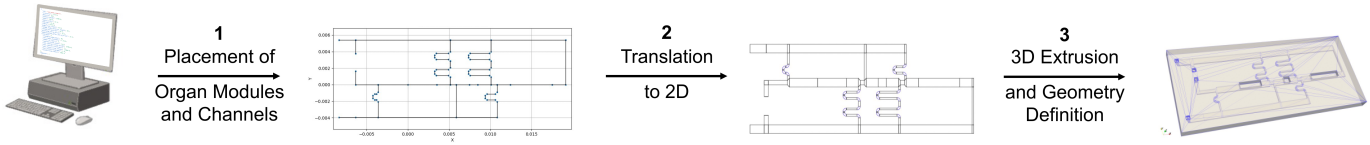

(a) Module and chip definitions. (b) Initial design. (c) Channel network definition. (d) 3D geometry.

Fig. 2: Flow of the automated design for microfluidic channel networks, partially created with biorender.com

where $Q_{organblood}$ $[\mathrm{m}^3/\mathrm{s}]$ is the standard blood flow through the organ, $Q_{totalblood}$ $[\mathrm{m}^3/\mathrm{s}]$ is the standard cardiac blood throughput, $V_{circ.fluid}$ $[\mathrm{m}^3]$ is the total volume of the circulating fluid flow, and V_{blood} $[\mathrm{m}^3]$ is the scaled down blood volume of a reference (e.g., a standard human male) proportional to the organ sizes on the multi-OoC.

It also includes the dilution of the communication molecules due to the larger circulating fluid volume compared to the blood volume [23]. In the current configuration, the dilution factor $V_{circ.fluid}/V_{blood}$ is set to 2. The channel branching (as also illustrated in Fig. 1c) allows to balance the flow rate to fulfill the requirements for shear stress as well as the physiological perfusion between organ modules.

Example 3. *Consider again the liver-on-chip module from above. The reported physiological perfusion of the liver of a standard human male is* $1450\,\mathrm{mL\,min^{-1}}$ *[30], the blood flow* $5600\,\mathrm{mL\,min^{-1}}$*. Together with a dilution factor of* 2 *, this results in a volume exchange of* $51.79\,\%$ *for the liver module. This percentage is then multiplied with the flow rate below the organ modules—resulting in the flow rate required in the connection channel. The flow rate of the discharge channel is the remaining flow* $(1-perf)\times Q$*, which results in* $48.21\% \times Q$ *and is equal to the flow rate of the supply channel.*

Utilizing the equations and constraints from above results in a formal specification for the entire multi-OoC design. Based on that, next we propose an approach using design automation methods for an automated generation of the desired design.

IV. Automated Design

Using the formal specification introduced above, a multi-OoC design can be realized in an automated fashion. For the organ module sizes, this can easily be accomplished by employing Eq. 1 and Eq. 2.

In contrast, the realization of the shear stress on the membranes, i.e., the flow rate below the membrane, and the microfluidic channel network for the circulating fluid that also realizes the physiological perfusion, requires some more steps in order to ensure that additional aspects such as pressure gradients and resistances are accounted for. Here, the position of all modules and channels, as well as the dimensions of those channels, need to be designed so that the correspondingly needed flow rates are realized. Additionally, this initial design needs to be translated into an actual geometry definition by first defining them as a 2D microfluidic channel network and, then, extruding them into a 3D geometry. To account for all that, an automated design flow comprising the following steps (and illustrated in Fig. 2) is proposed:

1) *Placement of Organ Modules and Channels*: First, all organ modules and channels need to be placed properly. This requires the determination of the coordinates where to place modules as well as the coordinates where channels start, end, or meet. For channels, also the respective/required lengths have to be determined. All that is accomplished by the following steps:
   a) *Initialization:* The required flow rates for all channels are determined.
   b) *Pressure Correction:* The pressure gradient, flow rate, and resistance of each channel are matched.
   c) *Channel Length Adaption:* Based on the information from Steps 1a and 1b, the lengths of all supply and discharge channels are determined. Then, these channels (with exactly the required length) are realized through meanders.
   d) *Offset Correction:* To properly place the resulting supply and discharge channels onto the chip, enough space between both is needed. To accommodate for that, a corresponding supply and discharge offset is applied, as shown in Fig. 3.
   The Steps 1b to 1d are carried out until no further pressure correction is necessary.
2) *Translation to 2D:* The initial design obtained by Step 1 is translated to a 2D network, including arcs, channel widths, and the transition between different channel widths.
3) *3D Extrusion and Geometry Definition:* The 2D channel network definition is extruded into a 3D geometry including two possible options:
   a) *Channel Positive Definition*: The channel network itself is defined as one coherent object with closed-off edges. This can be imported into simulation software tools.
   b) *Channel Negative/Chip Definition*: The chip geometry is defined including a hollow channel network with connections for the pump tubing as well as for organ modules. This can subsequently be fabricated.

Here, the user can define the number and type of each organ module, the resulting chip dimensions, and the connection to the pump tubing. The result is a valid multi-OoC geometry design as well as flow rate settings for the pumps. In the following, these steps are described in detail.

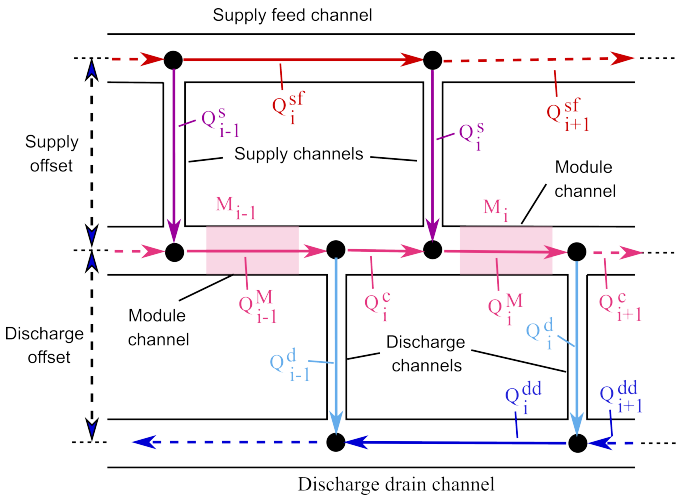

Fig. 3: Microfluidic channel network overview, including flow rates.

A. Placement of Organ Modules and Channels

In order to generate the initial design of a multi-OoC geometry, its components, specifically the organ modules and channels need to be placed. This requires the determination of the coordinates where organ modules are placed, including their respective sizes, as well as the coordinates where channels start, end, or meet. Additionally, the required channel lengths need to be calculated and accounted for. For this, the following steps are conducted:

1a) *Initialization.* First, the flow rates in all channels (cf. Fig. 3) are determined by calculating the required flow rate Q_i^M below each organ module M_i using Eq. 3. The flow rate Q_i^c of the connection between modules depends on the perfusion described in Eq. 4 and can be determined by $Q_i^c = perf \times Q_i^M$. The remaining flow rates can be determined by applying *Kirchhoff's current law* [33]: For each coordinate where multiple channels meet, the sum of the incoming flow rates equals the sum of the exiting flow. These junctions and the flow rates are illustrated for two modules in Fig. 3. Consequently, the equations

$$\begin{aligned} Q_i^s &= Q_i^M - Q_i^c, \\ Q_i^{sf} &= Q_{i+1}^{sf} + Q_i^s, \\ Q_i^d &= Q_i^M - Q_{i+1}^c, \text{ and} \\ Q_i^{dd} &= Q_{i+1}^{dd} + Q_i^d \end{aligned} \tag{5}$$

allow to determine the remaining flow rates. Then, the required flow rates for the inlet and outlet pumps (cf. Fig. 1a) are equal to the flow rates of the supply feed and discharge drain channel of the first module, i.e., Q_0^{sf} and Q_0^{dd}. Conversely, the flow rate of the connection channel Q_0^c in front of the first module defines the flow rate of the recirculation pump.

Second, the dimensions for each channel are fixed, i.e., the width w, height h, and length l are assigned. The module channel dimensions can be determined as described in Section III.

The other channels can be freely sized. However, a reasonable choice is to use a uniform channel height throughout the chip to facilitate subsequent fabrication. Additionally, the supply feed and discharge drain (horizontal channels) can be set to the same width as the module channel, while the vertical supply and discharge channels (cf. Fig. 3) should have a smaller diameter (e.g., $\frac{h}{w} = \frac{2}{3}$).

Finally, the channel resistances are computed. The resistance R of a rectangular channel is determined by the width w and height h of its cross-section, as well as its length l [34]. If $h \leq w$, and given the viscosity μ of the fluid, then a channel implements the resistance[2]

$$R = \frac{12\mu l}{1 - 0.63(\frac{h}{w})} \frac{1}{h^3 w}. \tag{6}$$

1b) *Pressure Correction.* Using the information from the previous step, the pressure gradients can be computed for every channel by employing the *Hagen-Poiseuille* equation, i.e.,

$$\Delta P = RQ, \tag{7}$$

where ΔP is the difference in pressure between two channel ends, R is the channel's resistance, and Q is the flow rate in the channel [33]. However, the channels may still violate *Kirchhoff's voltage law* [33] since, along any closed cycle of channels, the sum of oriented pressure gradients must be zero. To correct this violation, the pressure gradients of each module's vertical supply and discharge channels are manipulated by changing the channels' lengths until Kirchhoff's voltage law is satisfied.

This is illustrated in Fig. 4. More precisely, starting with the last organ module and iterating backwards, the supply and discharge channels are adjusted such that the sum of pressure gradients around each cycle is zero, i.e.,

$$\begin{aligned} \Delta P_i^s &= \Delta P_{i+1}^{s\prime} \\ \Delta P_i^d &= \Delta P_{i+1}^{d\prime}, \end{aligned} \tag{8}$$

where ΔP_i^s, ΔP_i^d are the pressure gradients along the supply and discharge channels of the module, and $\Delta P_{i+1}^{s\prime}$, $\Delta P_{i+1}^{d\prime}$ complete the cycle as indicated in Fig. 4 (marked by red arrows for the supply cycle and blue arrows for the discharge cycle). Such a pressure adjustment can be achieved in two ways:

1) If the pressure gradient needs to be larger, the channel length is increased l_i^s or l_i^d and, therefore, its resistance and pressure gradient.
2) If the pressure gradient needs to be smaller, it may not be possible to shorten the channel length in the same way. Instead, all channels of the succeeding modules are elongated such that the voltage law is satisfied in the same way.

By employing this procedure, it is ensured that the supply and discharge channels strictly increase and, thus, pressure correction can indeed be applied.

1c) *Channel Length Adaption.* The next task is to design the channel geometry. For this, based on the previous two steps, the channel lengths of all supply and discharge channels can be determined based on the pressure adjustment and the subsequently required additional length, since channel width

[2]This is an approximation for $\frac{h}{w} \to 0$, i.e., wide channels, which is the common case.

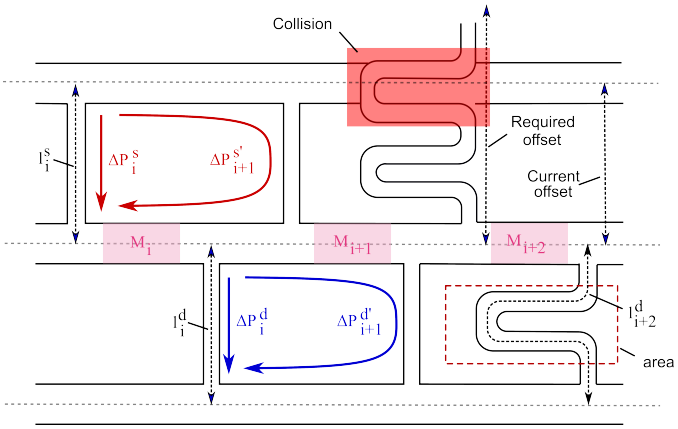

Fig. 4: Pressure gradient cycles and meanders.

and height are fixed. The exactly required length of each supply and discharge channel can be achieved by employing so-called *meander channels* [35]. In the red-dotted square in Fig. 4, a channel with a meander is depicted. It illustrates how meanders are used to achieve exactly the required channel length. The meanders have rounded bends for better fluid flow.

$1d$) *Offset Correction.* Finally, the resulting supply and discharge channels need to be placed onto the chip design. It has to be ensured that the resulting channels fit, since the addition of meanders as described in the previous step does not guarantee that the initial defined offset between organ modules and supply feed/discharge drain channel is sufficient. In fact, as illustrated in Fig. 4 (highlighted red), if the required channel length is too long, it will result in a collision of the supply or discharge channel and the supply feed/discharge drain channel. This is accommodated by increasing the supply and discharge offsets such that every meander has enough space to fit. However, after this correction, there may be supply/discharge channels that are too short to extend across the offset, and, therefore, their length and pressure gradient need to be adapted, after which further pressure correction is needed. Hence, Steps 1b to 1d are carried out until no further pressure correction is necessary.

Following the steps from above, all organ modules accounting for properly dimensioned tissue sizes are placed, and a microfluidic channel network for the circulating fluid is (automatically) designed, which connects them while at the same time realizing the desired flow and perfusion rate. A possible result is sketched in Fig. 2b. Now, this initial design definition needs to be further translated to an actual 2D geometry description. This requires the extension into an actual microfluidic channel network by introducing the defined channel widths, transitions between channels at intersections, and the inclusion of arcs. This translation takes place in Step 2.

B. 2D Translation

In order to translate the initial design to a 2D channel network, the created network description is used to generate an actual geometry definition, see Fig. 5. This is achieved by defining quads for each channel intersection, as well as the arcs

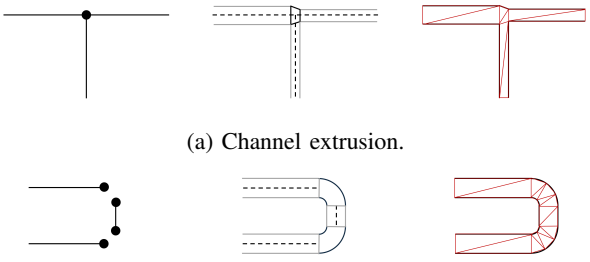

(a) Channel extrusion.

(b) Arc extrusion.

Fig. 5: 2D geometry extrusion and triangulation.

that are now created between the designated channel segments for better fluid flow. In Fig. 5a, the quads that bridge changes in channel width as well as accommodate for the connection of channels are depicted at an intersection of three channels. They are defined via the connected channels and their widths, creating a new quadrilateral that interconnects the channels. Since the absolute coordinate values of the start and end of channels stay the same, the channel lengths of the initial design and 2D network are identical.

In Fig. 5b, arcs are defined as 90° turns between the start and end of meandering supply and discharge channels. The effect of the rounded edges on the channel length is included in the geometry definition described above. Fig. 2c shows the resulting channel network definition.

The triangulation, i.e., the definition of the geometry as a collection of triangles, is technically created at a later point. However, for clarity, this process is described for the 2D geometry as well. In Fig. 5, the red lines symbolize the triangle definition of the shapes. Each quadrilateral in Fig. 5a is defined as two adjacent triangles, as depicted by the red lines. In Fig. 5b, this process is depicted for the arcs. Here, based on a defined resolution number, the arc is cut up into a finite number of triangles, which approximates an actual rounded shape. For clarity, a very low resolution number of arc triangles is depicted by the red lines in Fig. 5b.

Overall, this leads to a 2D channel network definition, as sketched in Fig. 2c. Now the geometry definition needs to be further translated to 3D.

C. 3D Extrusion and Geometry Definition

For the 3D geometry definition, the 2D geometry is extruded along the z-axis to create a 3D shape. Here, two options are possible, (1) the channel positive, i.e., the network geometry, or (2) the channel negative, i.e., the actual chip geometry, including the hollowed out channel network.

$3a$) *Channel Positive Definition* The channel positive geometry definition is created by extruding the 2D network directly and closing off the blunt edges, as well as all outward facing channel walls resulting in the microfluidic network geometry.

The triangulation of this geometry is analogous to that of the 2D geometry. The arcs are approximated using triangle shapes based on a defined resolution number. Quadrilaterals are defined by two adjacent triangles. The geometry definition is especially useful for subsequent simulations, as the result can be directly uploaded to most simulation software tools.

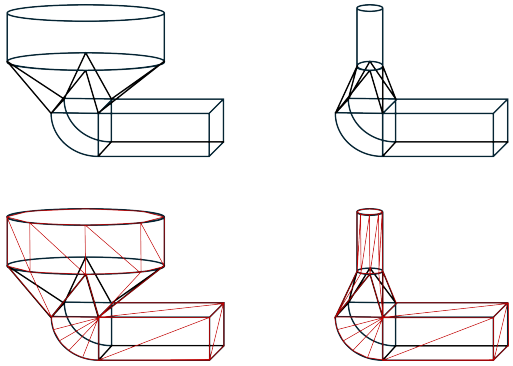

Fig. 6: Pump connections.

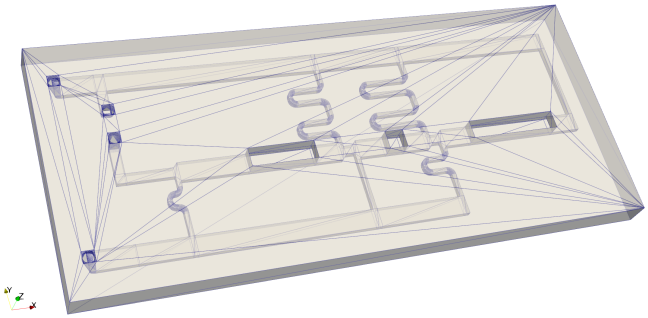

Fig. 7: Resulting 3D model.

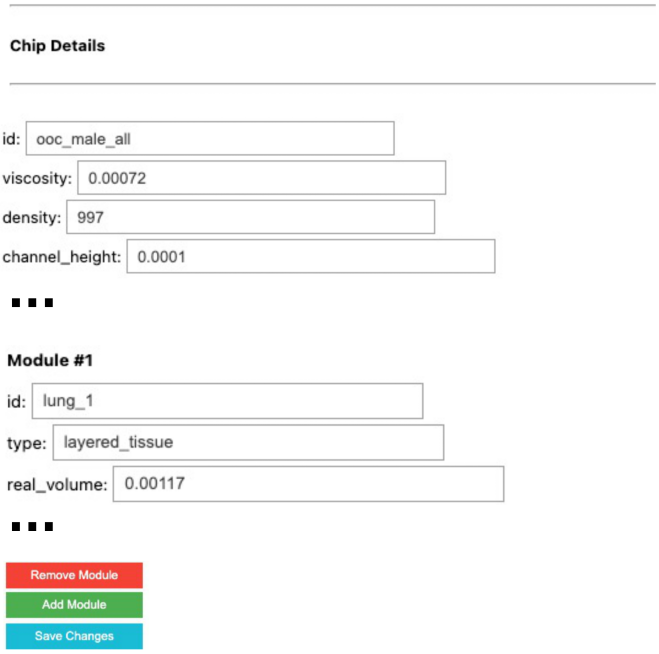

Fig. 8: Jupyter Notebook interface for the definition of chip dimensions and organ modules.

For example, for the commercial simulator COMSOL, the resulting geometry can directly be included via the geometry import. For the open-source simulator OpenFOAM, the geometry needs to be translated to an ASCII *.stl* format, which can easily be achieved via various libraries or tools. Here, specific walls can also be defined as inlets or outlets. For the mesh generation, first a block mesh needs to be generated that is fine enough to capture the details of the channel network. Then, *snappyHexMesh* can be used to snap the mesh to the desired geometry. We recommend activating the *castellatedMesh* and leave *snap* and *addLayers* deactivated. The closed-off edges allow for boundary definitions at the inlets and outlets.

3*b*) *Channel Negative/Chip Definition* For the channel negative, the chip surrounding is included in the geometry. First, the channel network is extruded. This time, the microfluidic channel network is left open at the designated connections to the pumps. Then the chip geometry is defined. Its dimensions are user defined and based on the required distance to the channel network that is housed inside the chip. Additionally, the connections to the pump tubing can be defined by the user to fit the available tubing and are automatically added to the geometry. In Fig. 6, pump connections based on a large or small tubing connection are depicted. The radius of the connection can be defined as an input, and for a seamless transition of the tubing to the channel network, arcs are employed.

The triangulation is analogous to the previously described method of cutting quadrilaterals into two triangles and defining rounded corners using a finite number of triangles.

For the organ tanks, the space for them (above the dedicated channel) is caved out to be able to plug in, e.g., a transwell or another module for the organ tissues.

In Fig. 2d and, in a more detailed fashion, in Fig. 7, the resulting geometry, including the hollow channel network, the chip dimensions, the connections for the pump tubing, and the organ tank openings, are depicted.

The channel negative definition can be directly fabricated, either by uploading it into a 3D printer software or by sending it to manufacturers for other forms of fabrication. The results are shown in the next section.

Overall, based on the formal specification of a multi-OoC, a design for the microfluidic channel network, organ module openings, and pump connections tailored to the predefined input are automatically created. The proposed approach generates several geometry definitions: In 2D for better visualization and in 3D, a positive channel network definition as well as a negative channel definition for subsequent analyses using simulations or fabrication, respectively.

V. Application and Evaluation

The described method has been implemented as a python script that automatically solves the requirements of the described formal specification of a multi-OoC geometry in negligible runtime and, hence, realizes a design of the desired devices automatically through the push of a button. In this section, we briefly describe the resulting tool and, afterwards, demonstrate how it can be used for simulation and fabrication.

A. Resulting Tool

The resulting tool covering the described automated design for multi-OoC geometries and an interactive step-by-step tutorial (provided through a *Jupyter Notebook*) are available at

TABLE I: Overview of organ modules for different sexes and organs, including properties derived from human organs like volume, mass, and blood perfusion rates

	Lung		Brain		Liver		Kidney	Gut	Adipose
	♀	♂	♀	♂	♀	♂	♂	♂	Tissue ♂
Type	layered	layered	round	round	layered	layered	layered	layered	layered
Volume [m^3]	$1.62e{-3}$	$1.17e{-3}$	$1.18e{-3}$	$1.45e{-3}$	$1.20e{-3}$	$1.69e{-3}$	$2.80e{-4}$	$1.65e{-3}$	$1.00e{-2}$
Mass [kg]	0.64	1	1.23	1.4	1.29	1.8	0.31	1.2[b]	9
No. of Layers	2	2			20[a]	20[a]	1	5	20
Blood flow [m^3/s]	$1.00e3$[c]	$1.00e3$[c]	$7.00e2$	$7.00e2$	$1.45e3$	$1.45e3$	$1.24e3$	$1.10e3$	$2.60e2$
Perfusion [%]	36	36	25	25	51	51	44	39	16.25[d]
Reference	[27]	[30]	[27]	[30]	[27]	[30]	[30]	[30]	[30], [36]

[a] Based on the thickness of 150 µm reported in [29]. [b] Based on the GI tract in [28]. [c] Chosen arbitrarily. [d] Size and perfusion are adapted to reduce compartment size while increasing the exposure to the fluid flow, calculated using [36]. ♀: female; ♂: male

TABLE II: Reference values used in the design method [30]

Reference values	
Mass [kg]	♀: 65 ; ♂: 70
Cell layer thickness[a] [m]	$7.50e{-6}$
Layered tissue width [m]	$1.00e{-3}$
Round tissue radius [m]	$2.50e{-4}$
Blood flow [m^3/s]	$5.60e3$
Dilution factor	2

[a] Can be adapted separately for each organ module. ♀: female; ♂: male

https://github.com/cda-tum/mmft-ooc-designer. There, a number of example organ combinations, which are also listed in Table I, and reference values, which are listed in Table II, are provided in the architectures directory.

The tutorial guides the user through the process of defining the required multi-OoC and exporting the resulting geometry files without the need for direct code interaction. In Step 1, the necessary scripts and modules are installed and imported. In Step 2, the definitions of the chip and the organ modules are specified. The interface for the input is partly depicted in Fig. 8. There, one of the provided templates that is based on literature examples (cf. Table I), can be directly used or altered according to the user's specific needs. In the next step, the chip is automatically designed. Then the user can decide on a channel negative or channel positive geometry definition, as well as define the sizes of the chip and pump connections. The geometry is generated by a translation to 2D and, subsequently, an extrusion to 3D. Finally, the results are generated in a "push-button" fashion, including plots and visualizations like the examples depicted in Fig. 2. The results of the tutorial are saved locally and can be directly used for further research.

Alternatively, the open-source python script can be used via the command line. The resulting geometry definitions are locally stored and can immediately be used in simulations, fabrication, and further research.

B. Generated Designs

In order to demonstrate the applicability and validity of the proposed automated design for multi-OoC geometries, we used the resulting tool described above to automatically generate various multi-OoC designs. In Table I, the values from literature that were used as examples are listed. This does not constitute a comprehensive library of organ modules that can be included but rather a list of examples to showcase the capabilities of the proposed tool. At the same time, individual organ modules can be included as well, based on the needs of the user. To this end, different use cases have been considered, from which a corresponding specification has been derived as described in Section III and, afterwards, *automatically* realized as described in Section IV.

More precisely, we considered four examples of multi-OoCs inspired by real-world examples with predefined organ arrangements and organ tissue types, as well as four generic examples in order to demonstrate the scalability of the approach. This includes combinations of a barrier tissue like the lung or the gastro-intestinal tract (gi-tract) for drug uptake [10], [15] with the liver, which plays a major role in the body's metabolism [37] and the brain, as it differs the most between humans and other animals [2]. Specifically, the female and male sex in an multi-OoC for a combination of lung, liver, and brain are represented by the *male_simple* and *female_simple* use cases. In Table I, the reference values for these are listed. The same combination with the gastro-intestinal tract as a barrier tissue, instead of the lung, is represented by the *male_gi_tract* use case. Finally, the kidney is included in the the *male_kidney* use case, allowing for the investigation of potential side effects on this organ [38]. Furthermore, four generic and larger use cases with liver tissue were considered (denoted by *generic1* to *generic4*).

In practical applications, the use of more modules requires significant resources and, in the foreseeable future, the combination of a few modules will remain the norm [18]. Under these conditions, the runtimes of the design tool are negligible (i.e., less than 1 s), and the method's efficiency and scalability exceed current requirements.

For each of the described use cases, a variation of certain parameters has been applied, i.e., each basic multi-OoC use case was instantiated for several viscosity values $\mu \in \{7.2e{-4}, 9.3e{-4}, 1.1e{-3}, 3e{-3}\}[\mathrm{Pa\,s}]$ [32], shear stress values $\tau \in \{12e{-1}, 15e{-1}, 20e{-1}\}[\mathrm{Pa}]$ [39], and spacing values (minimum distance between channels) $\{0.5e{-3}, 1e{-3}, 1.5e{-3}\}[\mathrm{m}]$. In total, this led to 288 multi-OoC geometry designs, which have been generated in negligible runtime (i.e., less than 1 s). All use cases are available

TABLE III: Summary of obtained results

Use case	Modules	Deviation [%] in perfusion		Deviation [%] in flow rate	
		avg	max	avg	max
male_simple	3	1.01	3.71	0.91	2.50
female_simple	3	1.62	3.29	1.98	3.50
male_gi_tract	3	0.91	3.70	0.54	1.21
male_kidney	4	3.07	11.87	0.96	3.55
generic1	5	2.70	5.80	1.61	3.72
generic2	6	1.50	4.40	1.36	3.71
generic3	7	2.21	8.13	2.06	6.53
generic4	8	1.53	5.29	1.82	5.52

at https://github.com/cda-tum/mmft-ooc-designer and can be easily replicated as the tool and the templates are accessible online.

C. Simulation

The resulting designs described in the previous Section V-B were simulated using *Computational Fluid Dynamics* (CFD) simulations to validate whether they work as intended.

More precisely, in our evaluations, we used the open-source CFD simulator OpenFOAM v10 [40]. The computational domain consisted of the channels defined by the proposed design method. The inlet values were set to the constant velocities that were calculated by the method (and stored as the "pump" flowrates in the resulting *.json* file). The outlets were defined with a zero-gradient pressure. The initial flow field was set to a uniform velocity distribution with zero turbulence, using a *Newtonian* transport model. The *simpleFoam* solver was employed. The time step was dynamically adjusted to maintain a *Courant number* below 0.5. In addition, several function objects were employed for automatic post-processing of simulation data.

The obtained results are summarized in Table III. Here, the first two columns provide the identifier of the use case as well as the respectively considered number of organ modules. Afterwards, the relative deviations (in %) in perfusion rates and module flow rates between the specification and the resulting design (as obtained by the CFD simulation) are provided (note that we aggregated these values for all instances and provide the average deviation and the maximal, i.e., worst-case, deviation in Table III).

The results clearly show how accurately the proposed method realizes the desired multi-OoC geometry designs in most of the cases. There are a few single instances in which the deviation gets significant (e.g., for *male_kidney* with a deviation of up to 11.87 % in the worst case). This is because, after all, for an efficient design automation method, simplifications such as using approximate formulas for certain physical quantities (e.g., Eq. 6) cannot be avoided (which is why every design should be simulated before further consideration). However, even in these cases, manually adjusting an automatically generated design is still substantially better than doing the entire design manually.

Moreover, in the vast majority of use cases, the deviations are negligible. In fact, on average, the deviations are less than

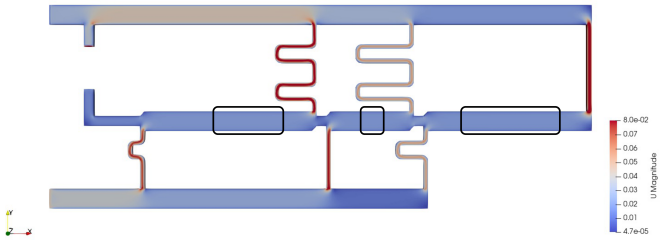

Fig. 9: Simulation result.

3 % (even including the worst cases)—which is within the typical tolerances applied in microfluidics and, hence, more than acceptable for an automated microfluidic design. This clearly confirms that, on a broad spectrum of multi-OoCs, the proposed method is capable of (automatically) generating the desired designs.

To explicitly include a resulting design, Fig. 9 shows the resulting design (as well as the simulation result) of an instance of the *male_simple* use case. Here, the color gradient illustrates the fluid velocities, which shows that the velocities and, therefore, the flow rates are approximately the same in each module channel (marked by boxes). More precisely, the measured flow rates for Modules 1, 2, and 3 are 8.09, 8.06, and 8.04 $[\mathrm{e}{-9}\mathrm{m}^3/\mathrm{s}]$, respectively, whereas the chip was intended to have a flow rate of 8.06 $[\mathrm{e}{-9}\mathrm{m}^3/\mathrm{s}]$ in all modules—resulting in a deviation between the specification and the resulting design of 0.36 %, 0.07 %, and 0.34 %, respectively. Conversely, the measured perfusion rates for each module deviate from the intended values by 0.35 %, 0.91 %, and 0.53 %. As discussed above, the corners of the the supply and discharge channels that include meanders were rounded to achieve a better flow profile, and the flow rates had overall lower deviations from the desired results compared to the preliminary version of this work [14].

Overall, these evaluations confirm that the designs, which have been *automatically* generated with the approach proposed in this work, indeed work as desired.

D. Fabrication

Lastly, to demonstrate that the results generated by the proposed approach can directly be used as input for the fabrication of the desired design, we also fabricated one of the obtained multi-OoC geometries.

For this, a commercially available stereolithography (SLA) 3D printer (Formlabs, Form 3) was used. The automatically created output of the proposed approach already has the correct file format (*.stl*) for the subsequent printing. In Fig. 10, the fabrication steps and the resulting chip, including a representation of the circulating fluid flow, are depicted. The microfluidic network in the chip is filled with water colored with ink. The red color represents the fresh media supply, which is then depleted by the organs in the tanks. This is visualized by the blue colored water.

The printed chip geometry, which was designed based on the use case that is also used as a representative in the simulation,

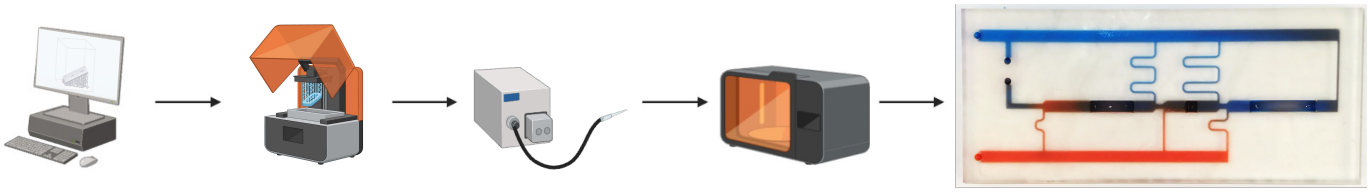

(a) Load .stl. (b) Print chip. (c) Clean the channels. (d) Cure print. (e) 3D printed chip, increased size, filled with water colored with ink.

Fig. 10: Chip fabrication using 3D printer, partially created with biorender.com.

was fabricated, as depicted in Fig. 10, based on the following fabrication steps:

(a) The 3D geometry, based on the provided templates, was imported into the printing software (PreForm), and scaled up by factor 4. This scale up was necessary to achieve clear and unclogged channels and can most likely be avoided by using customized 3D printers or other means of fabrication.
(b) The chip was printed using a clear resin at 35°C.
(c) The print was washed in Tripropylenglykol-monomethylether (TPM, 3Dmensionals) and water. Furthermore, a pressure pump was used to clean the channels from the printing resin. The residual TPM was washed of the printed chip using water, and it was left to dry.
(d) After drying completely, it was cured at 60°C for 15 min in an UV curing device (Form Cure, Formlabs). Lastly, the scaffolding was removed.

The goal of the fabrication process was to demonstrate the flexibility and applicability of the automatically created designs by our tool rather than the production of the physical chip itself. Although the fabrication process needed scaling of the design to be able to achieve unclogged channels, the process of uploading and initiating the print was uncomplicated and efficient. This highlights the potential of an integration of the design tool into manufacturing workflows.

When fabricating the chip for cell experiments, regardless of the fabrication method, several factors must be considered [8], [41]: (1) the chip material should be transparent, or at least parts of the chip must support optical monitoring, providing a clear view of the channels and organ tanks; (2) the chip material needs to be biocompatible to ensure cell viability; (3) the chip material's permeability to oxygen and uptake of drugs into the periphery should be considered [1], [42]; (4) measures for a smooth experimental set-up like clamps and to prevent potential leakage at the connection points should be taken. These considerations are left for future experiments, as the focus of this work is the design of the multi-OoC.

Overall, the applicability of results automatically generated by the proposed approach to fabrication is confirmed.

VI. Conclusions

In this work, we proposed an automated design approach for multi-Organ-on-Chip geometries. To this end, we first derived organ module specifications from literature and created a subset of module templates that can be combined, adapted, and expanded to create the desired combination of organ modules. Afterwards, an automatic approach was introduced that masters the orchestration of numerous aspects such as the size of organ modules, the required shear stress on membranes, the dimensions and geometry of channels, pump pressures, etc. Finally, the obtained design is automatically drawn as a 2D image, and exported as a 3D network definition ready for simulation and fabrication. By doing so, the design of multi-OoCs, which, thus far, was executed manually, has been automated.

Eventually, the resulting method accounts for physiological parameters and automatically generates a corresponding microfluidic channel network geometry. This 3D definition can be uploaded to most simulation software tools. Additionally, we define a chip definition, including pump and organ tank connections where tubing, or tanks (e.g., transwells) can be included or directly plugged in. This chip design can be exported as an *.stl* file and be directly 3D printed or sent to a manufacturer.

The applicability and validity of the generated designs have been evaluated using instances inspired by real-world use cases and CFD simulations, respectively. To the best of our knowledge, this is the first attempt towards design automation for multi-OoCs—providing a fundamental basis for the further development of automatic design methods for multi-OoCs. The resulting tool and a corresponding tutorial are available at https://github.com/cda-tum/mmft-ooc-designer.

Acknowledgment

This work has partially been supported by the Austrian Research Promotion Agency (FFG) project AUTOMATE (project number: 890068) as well as by BMK, BMDW, and the State of Upper Austria in the frame of the COMET Programme managed by FFG.

References

[1] K. Ronaldson-Bouchard, D. Teles, K. Yeager, D. N. Tavakol, Y. Zhao *et al.*, "A multi-organ chip with matured tissue niches linked by vascular flow," *Nature Biomedical Engineering*, vol. 6, no. 4, pp. 351–371, 2022.
[2] S. Kofman, N. Mohan, X. Sun, L. Ibric, E. Piermarini *et al.*, "Human mini brains and spinal cords in a dish: Modeling strategies, current challenges, and prospective advances," *Journal of Tissue Engineering*, vol. 13, 2022.
[3] A. Tajeddin and N. Mustafaoglu, "Design and fabrication of organ-on-chips: Promises and challenges," *Micromachines*, vol. 12, no. 12, p. 1443, 2021.

[4] H. Sun, Y. Jia, H. Dong, D. Dong, and J. Zheng, "Combining additive manufacturing with microfluidics: an emerging method for developing novel organs-on-chips," *Current Opinion in Chemical Engineering*, vol. 28, pp. 1–9, 2020.

[5] H.-G. Yi, H. Lee, and D.-W. Cho, "3D printing of organs-on-chips," *Bioengineering*, vol. 4, no. 4, p. 10, 2017.

[6] M. R. Haque, C. R. Wessel, D. D. Leary, C. Wang, A. Bhushan *et al.*, "Patient-derived pancreatic cancer-on-a-chip recapitulates the tumor microenvironment," *Microsystems & Nanoengineering*, vol. 8, no. 1, p. 36, 2022.

[7] K. Ronaldson-Bouchard and G. Vunjak-Novakovic, "Organs-on-a-chip: A fast track for engineered human tissues in drug development," *Cell Stem Cell*, vol. 22, no. 3, pp. 310–324, 2018.

[8] C. M. Leung, P. de Haan, K. Ronaldson-Bouchard, G.-A. Kim, J. Ko *et al.*, "A guide to the organ-on-a-chip," *Nature Reviews Methods Primers*, vol. 2, no. 1, p. 33, 2022.

[9] R. Prantil-Baun, R. Novak, D. Das, M. R. Somayaji, A. Przekwas *et al.*, "Physiologically based pharmacokinetic and pharmacodynamic analysis enabled by microfluidically linked organs-on-chips," *Annual Review of Pharmacology and Toxicology*, vol. 58, no. 1, pp. 37–64, 2018.

[10] M. B. Esch, H. Ueno, D. R. Applegate, and M. L. Shuler, "Modular, pumpless body-on-a-chip platform for the co-culture of GI tract epithelium and 3d primary liver tissue," *Lab on a Chip*, vol. 16, no. 14, pp. 2719–2729, 2016.

[11] Y. Baert, I. Ruetschle, W. Cools, A. Oehme, A. Lorenz *et al.*, "A multi-organ-chip co-culture of liver and testis equivalents: a first step toward a systemic male reprotoxicity model," *Human Reproduction*, vol. 35, no. 5, pp. 1029–1044, 2020.

[12] Y. S. Zhang, J. Aleman, S. R. Shin, T. Kilic, D. Kim *et al.*, "Multisensor-integrated organs-on-chips platform for automated and continual in situ monitoring of organoid behaviors," *Proceedings of the National Academy of Sciences*, vol. 114, no. 12, pp. E2293–E2302, 2017.

[13] P. Loskill, S. G. Marcus, A. Mathur, W. M. Reese, and K. E. Healy, "μorgano: A Lego®-like plug & play system for modular multi-organ-chips," *PLoS One*, vol. 10, no. 10, p. e0139587, 2015.

[14] M. Emmerich, P. Ebner, and R. Wille, "Design automation for organs-on-chip," in *Design, Automation and Test in Europe (DATE)*. IEEE, 2024.

[15] A. Artzy-Schnirman, N. Hobi, N. Schneider-Daum, O. T. Guenat, C.-M. Lehr *et al.*, "Advanced in vitro lung-on-chip platforms for inhalation assays: From prospect to pipeline," *European Journal of Pharmaceutics and Biopharmaceutics*, vol. 144, pp. 11–17, 2019.

[16] D. E. Ingber, "Human organs-on-chips for disease modelling, drug development and personalized medicine," *Nature Reviews Genetics*, vol. 23, no. 8, pp. 467–491, 2022.

[17] A. Chramiec, D. Teles, K. Yeager, A. Marturano-Kruik, J. Pak *et al.*, "Integrated human organ-on-a-chip model for predictive studies of anti-tumor drug efficacy and cardiac safety," *Lab on a Chip*, vol. 20, no. 23, pp. 4357–4372, 2020.

[18] C. D. Edington, W. L. K. Chen, E. Geishecker, T. Kassis, L. R. Soenksen *et al.*, "Interconnected Microphysiological Systems for Quantitative Biology and Pharmacology Studies," *Scientific Reports*, vol. 8, no. 1, p. 4530, 2018.

[19] H. E. Abaci and M. L. Shuler, "Human-on-a-chip design strategies and principles for physiologically based pharmacokinetics/pharmacodynamics modeling," *Integrative Biology*, vol. 7, no. 4, pp. 383–391, 2015.

[20] T.-P. Tao, I. Maschmeyer, E. L. LeCluyse, E. Rogers, K. Brandmair *et al.*, "Development of a microphysiological skin-liver-thyroid chip3 model and its application to evaluate the effects on thyroid hormones of topically applied cosmetic ingredients under consumer-relevant conditions," *Frontiers in Pharmacology*, vol. 14, p. 1076254.

[21] A. Peirsman, E. Blondeel, T. Ahmed, J. Anckaert, D. Audenaert *et al.*, "MISpheroID: a knowledgebase and transparency tool for minimum information in spheroid identity," *Nature Methods*, vol. 18, no. 11, pp. 1294–1303, 2021.

[22] D. Huh, B. D. Matthews, A. Mammoto, M. Montoya-Zavala, H. Y. Hsin *et al.*, "Reconstituting Organ-Level Lung Functions on a Chip," *Science*, vol. 328, no. 5986, pp. 1662–1668, 2010.

[23] J. P. Wikswo, E. L. Curtis, Z. E. Eagleton, B. C. Evans, A. Kole *et al.*, "Scaling and systems biology for integrating multiple organs-on-a-chip," *Lab on a Chip*, vol. 13, no. 18, p. 3496, 2013.

[24] K. J. Blose, J. T. Krawiec, J. S. Weinbaum, and D. A. Vorp, "Bioreactors for tissue engineering purposes," in *Regenerative Medicine Applications in Organ Transplantation*. Elsevier, 2014, pp. 177–185.

[25] E. Roux, P. Bougaran, P. Dufourcq, and T. Couffinhal, "Fluid shear stress sensing by the endothelial layer," *Frontiers in Physiology*, vol. 11, p. 861, 2020.

[26] J. R. Alvarez-Dominguez and D. A. Melton, "Cell maturation: Hallmarks, triggers, and manipulation," *Cell*, vol. 185, no. 2, pp. 235–249, 2022.

[27] D. K. Molina and V. J. M. DiMaio, "Normal Organ Weights in Women: Part II—The Brain, Lungs, Liver, Spleen, and Kidneys," *American Journal of Forensic Medicine & Pathology*, vol. 36, no. 3, pp. 182–187, 2015.

[28] P. S. Price, R. B. Conolly, C. F. Chaisson, E. A. Gross, J. S. Young *et al.*, "Modeling Interindividual Variation in Physiological Factors Used in PBPK Models of Humans," *Critical Reviews in Toxicology*, vol. 33, no. 5, pp. 469–503, 2003.

[29] M. G. Christensen, C. Cawthorne, C. E. Dyer, J. Greenman, and N. Pamme, "Investigating oxygen transport efficiencies in precision-cut liver slice-based organ-on-a-chip devices," *Microfluidics and Nanofluidics*, vol. 25, no. 4, p. 35, 2021.

[30] B. Davies and T. Morris, "Physiological parameters in laboratory animals and humans," *Pharmaceutical Research*, vol. 10, no. 7, pp. 1093–1095, 1993.

[31] W. Wei, Y.-S. Pu, X.-K. Wang, A. Jiang, R. Zhou *et al.*, "Wall shear stress in portal vein of cirrhotic patients with portal hypertension," *World Journal of Gastroenterology*, vol. 23, no. 18, p. 3279, 2017.

[32] C. Poon, "Measuring the density and viscosity of culture media for optimized computational fluid dynamics analysis of in vitro devices," *Journal of the Mechanical Behavior of Biomedical Materials*, vol. 126, p. 105024, 2022.

[33] A. Grimmer, W. Haselmayr, and R. Wille, "Automated dimensioning of Networked Labs-on-Chip," *Trans. on Computer-Aided Design of Integrated Circuits and Systems*, pp. 1216–1225, 2018.

[34] H. Bruus, *Theoretical microfluidics*. Oxford university press Oxford, 2008, vol. 18.

[35] A. Grimmer, P. Frank, P. Ebner, S. Häfner, A. Richter *et al.*, "Meander designer: Automatically generating meander channel designs," *Micromachines – Journal of Micro/Nano Sciences, Devices and Applications*, vol. 9, no. 12, p. 625, 2018.

[36] A. D. Martin, M. Z. Daniel, D. T. Drinkwater, and J. P. Clarys, "Adipose tissue density, estimated adipose lipid fraction and whole body adiposity in male cadavers," *International Journal of Obesity and Related Metabolic Disorders: Journal of the International Association for the Study of Obesity*, vol. 18, no. 2, pp. 79–83, 1994.

[37] R. Vaja and M. Rana, "Drugs and the liver," *Anaesthesia & Intensive Care Medicine*, vol. 21, no. 10, pp. 517–523, 2020.

[38] M. J. Wilmer, C. P. Ng, H. L. Lanz, P. Vulto, L. Suter-Dick *et al.*, "Kidney-on-a-chip technology for drug-induced nephrotoxicity screening," *Trends in Biotechnology*, vol. 34, no. 2, pp. 156–170, 2016.

[39] D. C. Fernandes, T. L. Araujo, F. R. Laurindo, and L. Y. Tanaka, "Chapter 7 - hemodynamic forces in the endothelium: From mechanotransduction to implications on development of atherosclerosis," in *Endothelium and Cardiovascular Diseases*, P. L. Da Luz, P. Libby, A. C. Chagas, and F. R. Laurindo, Eds. Academic Press, 2018, pp. 85–95.

[40] H. Jasak, "Openfoam: open source CFD in research and industry," *International Journal of Naval Architecture and Ocean Engineering*, vol. 1, no. 2, pp. 89–94, 2009.

[41] V. S. Shirure and S. C. George, "Design considerations to minimize the impact of drug absorption in polymer-based organ-on-a-chip platforms," *Lab on a Chip*, vol. 17, no. 4, pp. 681–690, 2017.

[42] A. W. Auner, K. M. Tasneem, D. A. Markov, L. J. McCawley, and M. S. Hutson, "Chemical-PDMS binding kinetics and implications for bioavailability in microfluidic devices," *Lab on a Chip*, vol. 19, no. 5, pp. 864–874, 2019.

Maria Emmerich received her Master's degree in biotechnology from the Technical University of Berlin, Germany, in 2022. Currently, she is a Ph.D. student at the Technical University of Munich. Her main research interest are design automation and simulation for microfluidics and organs-on-chips.

Philipp Ebner received his Master's degree in computer science from the Johannes Kepler University Linz, Austria, in 2021. Currently, he is a Ph.D. student at the Institute for Integrated Circuits at the Johannes Kepler University. His main research interest is design automation for microfluidics.

Robert Wille (M'06–SM'15) is a Full and Distinguished Professor at the Technical University of Munich, Germany, and Chief Scientific Officer at the Software Competence Center Hagenberg, Austria. He received the Diploma and Dr.-Ing. degrees in Computer Science from the University of Bremen, Germany, in 2006 and 2009, respectively. Since then, he worked at the University of Bremen, the German Research Center for Artificial Intelligence (DFKI), the University of Applied Science of Bremen, the University of Potsdam, and the Technical University Dresden. From 2015 until 2022, he was Full Professor at the Johannes Kepler University Linz, Austria, until he moved to Munich. His research interests are in the design of circuits and systems for both conventional and emerging technologies. In these areas, he published more than 400 papers and served in editorial boards as well as program committees of numerous journals/conferences such as TCAD, ASP-DAC, DAC, DATE, and ICCAD. For his research, he was awarded, e.g., with Best Paper Awards, e.g., at TCAD and ICCAD, an ERC Consolidator Grant, a Distinguished and a Lighthouse Professor appointment, a Google Research Award, and more.